Micropower Circuits for Bidirectional Wireless Telemetry in Neural Recording Applications

Nathan M. Neihart, *Student Member, IEEE,* and Reid R. Harrison*, *Member, IEEE*

***Abstract*—State-of-the art neural recording systems require electronics allowing for transcutaneous, bidirectional data transfer. As these circuits will be implanted near the brain, they must be small and low power. We have developed micropower integrated circuits for recovering clock and data signals over a transcutaneous power link. The data recovery circuit produces a digital data signal from an ac power waveform that has been amplitude modulated. We have also developed an FM transmitter with the lowest power dissipation reported for biosignal telemetry. The FM transmitter consists of a low-noise biopotential amplifier and a voltage controlled oscillator used to transmit amplified neural signals at a frequency near 433 MHz. All circuits were fabricated in a standard 0.5-μm CMOS VLSI process. The resulting chip is powered through a wireless inductive link. The power consumption of the clock and data recovery circuits is measured to be 129 μW; the power consumption of the transmitter is measured to be 465 μW when using an external surface mount inductor. Using a parasitic antenna less than 2 mm long, a received power level was measured to be -59.73 dBm at a distance of one meter.**

***Index Terms*—Biotelemetry, low-power CMOS circuits, RF telemetry, transcutaneous data link, transmitter.**

I. Introduction

With advances in integrated circuit technology and the development of new biocompatible materials, biomedical implants are becoming more common. Modern MEMS technology has led to the development of large-scale neural recording devices such as microelectrode arrays containing as many as 100 independent electrodes [1], [2]. These arrays have many potential uses in both the scientific and clinical realms.

A current limitation of this technology is the way in which recorded neural signals are transferred from the recording device, which is ideally implanted in the body, to signal processing equipment used for scientific or neuroprosthetic applications. In most modern neuroscience laboratories, wires are used to connect the implanted recording device to external amplification and signal processing equipment. There are two main problems with the use of transcutaneous cables: (1) the risk of infection, and (2) noise pickup due to the high impedance and low signal levels associated with neural recording.

Manuscript received August 2, 2004; revised February 20, 2005. This work was supported in part by the National Science Foundation (NSF) under CAREER Grant ECS-0134336. *Asterisk indicates corresponding auhtor.*

N. M. Neihart was with the University of Utah, Salt Lake City, UT 84112 USA. He is now with the Department of Electrical Engineering, University of Washington, Seattle, WA 98195 USA.

*R. R. Harrison is with the Department of Electrical and Computer Engineering, University of Utah, Salt Lake City, UT 84112 USA (e-mail: harrison@ece.utah.edu).

Digital Object Identifier 10.1109/TBME.2005.856247

One solution to these problems is to replace the cables with a wireless transmitter powered through a magnetic transcutaneous link. Such a system eliminates any cables protruding through the skin, reducing the chance of postoperative infections. A transmitter implanted near the electrode array also shortens the distance that the neural signal must travel over a wire, thus reducing a substantial source of noise. The transmitting system should also amplify the weak neural signals before transmission further improving the signal to noise ratio.

A wide variety of transmitters for telemetering biological signals have been previously reported [3]–[7]. However, these transmitters are not well suited for implantable neural recording applications. The circuits reported in [3]–[5] use a large number of discrete components, which makes these transmitters larger than the integrated solution detailed in this paper. The circuits reported in [6] and [7] are optical transmitters, and suffer from limited transmission distances (often in the millimeter range). Moreover, most of the previously mentioned transmitters use batteries as power supplies. These batteries have a finite lifetime and would require additional surgeries in order to be replaced. Even rechargeable batteries have a limited number of recharge cycles before they must be replaced.

In many medical applications, bidirectional wireless data transfer is necessary to transmit configuration data and a reference clock signal to the implant. In a neural recording device, the configuration data could be used to select which electrode should be actively recording, or which bank of amplifiers could be powered down to save energy. A clock signal is often necessary to synchronize the implant's telemetry with the outside circuitry.

In this paper, we present a low-power bidirectional telemetry system that is suitable for use in a fully implanted neural recording application. The system is capable of recovering a clock and data signal that is transmitted into the body, as well as transmitting amplified neural data out of the body. The entire system performs these operations while powered from a magnetic transcutaneous link. In Section II, we describe circuits for a wireless power and data link. In Section III, we present a low-power integrated FM transmitter. A discussion of the test setup and testing results, including a comparison of this work with other similar work, is given in Section IV. We summarize and draw conclusions in Section V.

II. Wireless Powered Data Link

A. Wireless Power Supply

Power is supplied to our circuits by means of a magnetic transcutaneous power link adapted from [8]. Component values

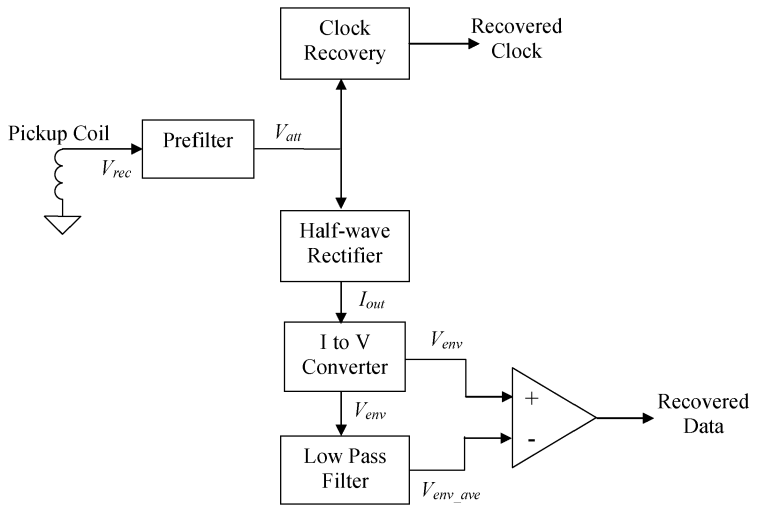

Fig. 1. Block diagram of the implantable clock and data recovery circuitry.

were modified to give an operating frequency of 1 MHz. The choice of operating frequency is a tradeoff between magnetic coupling, which increases with frequency, and power absorption into the skin, which also increases with frequency. A class E amplifier is used to drive a 10-cm diameter, 22-turn #200/38 Litz wire transmitting coil at 1 MHz ($L = 18\ \mu$H, $Q > 100$ at 1 MHz). The amplifier is capable of amplitude modulating the transmitted power waveform to encode data on the power link.

The ac signal is received with a 4-cm diameter coil consisting of four turns of 28 AWG wire ($L = 1.6\ \mu$H, $Q = 100$ at 1 MHz). The coils were separated by a distance of approximately 1 cm. Both coils were designed to have a reasonable size for implantable device applications. Little effort was placed into optimizing the magnetic link between transmitter and receiver in this work, but this topic has received considerable attention elsewhere [9]–[11].

The received ac signal is converted to a dc signal of the required magnitude by a bridge rectifier followed by an on-chip linear voltage regulator [12]. For ease of testing, the rectifier is currently an off-chip component, but could easily be fully integrated in the future [13]. The voltage regulator used has a dropout voltage of 1.4 V and provided a regulation of 647 ppm/V. As we will show in later sections, the overall power consumption of the integrated circuit is less than 1 mW. The class E power transmitter consumes approximately 2 W, resulting in an overall power transfer efficiency much less than 1%. This low efficiency results in large part from the inefficient coupling of the transmit and receive coils, and underscores the need for ultra-low-power implantable electronics.

B. Circuits for Clock and Data Recovery

Traditionally, data is either amplitude modulated or frequency modulated onto the power waveform that is used to power the implant [8], [11]–[15]. For this work, amplitude modulation was chosen over frequency modulation in order to reduce the complexity and power consumption of the implanted demodulation circuitry. Fig. 1 shows a block diagram of the proposed fully integrated system whose components are described below.

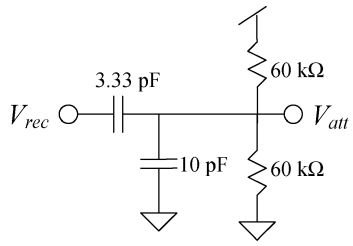

Fig. 2. Prefilter circuit used to attenuate the received power waveform and set the dc level to $V_{DD}/2$.

1) Prefilter: The received ac power waveform cannot be directly applied to the input of the clock and data recovery circuitry for two reasons. First, the magnitude of the ac signal can be greater than 10 V, and prolonged application of a signal of this magnitude could result in damage to, or even failure of, the inputs of the clock and data recovery circuitry. Second, an arbitrary dc offset can be present in the received power waveform. This offset could result in the saturation of the data recovery circuit and must be removed before further processing can take place. The prefilter is responsible for correcting both of these problems (see Fig. 2). The circuit consists of a capacitor voltage divider, which attenuates the received power waveform by a factor of four and removes any dc offset. Two resistors set the dc bias point to $V_{DD}/2$, where V_{DD} is the regulated on-chip power supply voltage.

2) Clock Recovery Circuit: An on-chip clock signal may be recovered from the transmitted power waveform. The clock recovery circuit consists of a Schmitt trigger followed by a master-slave D flip-flop as shown in Fig. 3. The Schmitt trigger is used to make the circuit more resistant to high frequency noise that may be present on the received power waveform. The D flip-flop guarantees a clock signal with a 50% duty cycle, regardless of the duty cycle of the received power waveform. The frequency of the recovered clock signal is one half the frequency of the received power waveform.

3) Data Recovery Circuit: Because data is amplitude modulated onto the received power signal, an amplitude demodulator

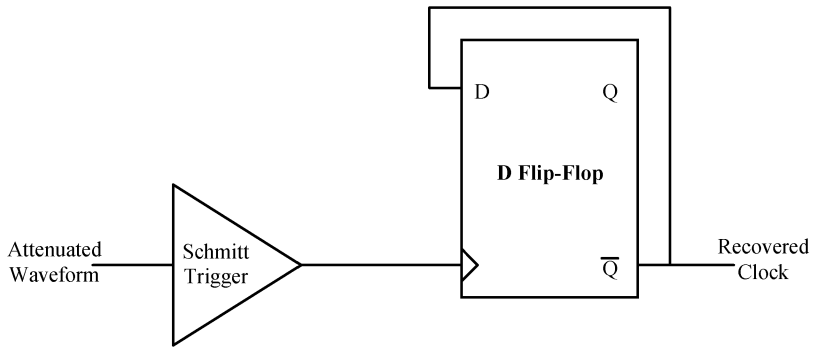

Fig. 3. Block diagram of the clock recovery circuit used in this work.

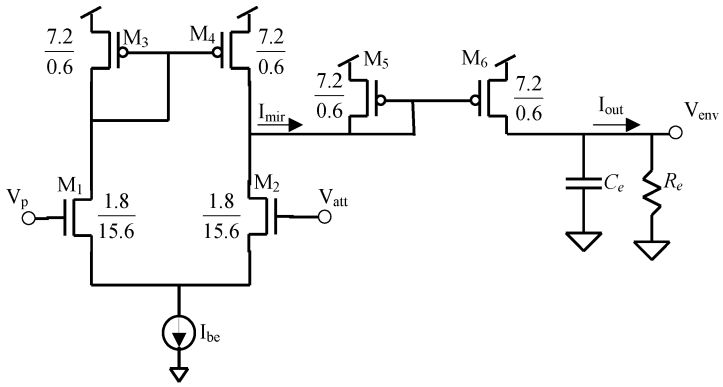

Fig. 4. Circuit schematic of the envelope detector used in the data recovery circuit. All dimensions are in microns. $R_e = 660$ kΩ and $C_e = 20$ pF.

is needed to recover the data. The data recovery circuitry consists of an envelope detector (half-wave rectifier and I-V converter), a low-pass filter, and a comparator (see Fig. 1). Fig. 4 shows the circuit schematic for the envelope detector. Transistors M_1-M_4 constitute a standard operational transconductance amplifier (OTA). This circuit takes a voltage input, V_{att} from the prefilter and produces a current output, I_{out}, that is proportional to V_{att}-V_p. The voltage V_p, is tied to a dc reference voltage. The bias current, I_{be} is set to 1 μA.

The addition of transistors M_5 and M_6 results in an output current that is a scaled, half-wave rectified version of the input voltage [16]. To illustrate this, consider the case where V_{att} is at a higher potential than V_p. The output voltage of the OTA will drop, allowing transistors M_5 and M_6 to conduct; hence, I_{mir} is mirrored to I_{out}. Conversely, if V_{att} is at a lower potential than V_p, the output voltage of the OTA approaches V_{DD} and turns off transistors M_5 and M_6. The result is an output current that is very close to zero.

The components R_e and C_e have values of 660 kΩ and 20 pF, respectively, and have been added to accomplish two tasks. First, they make up a low-pass filter with a cutoff frequency of approximately 12 kHz. This serves to filter out the 1-MHz carrier signal from the detected envelope. Second, the resistor acts as an I-V converter, converting the output current, I_{out}, to a voltage, V_{env}, for use by subsequent stages.

The detected envelope, V_{env}, can have a varying dc offset as well as varying amplitude. This variation could result in data reception errors if V_{env} were used directly as the recovered data signal. A possible solution to this problem would be to use a comparator with one of its inputs tied to a dc reference voltage and the other connected to V_{env}. The shortcoming of this solution is that the data would be lost (due to the output of the comparator saturating) if the dc reference voltage and the offset of the detected envelope differ by more than the amplitude V_{env}.

This circuit can be made more adaptable and robust by passing V_{env} through a low-pass filter with a very low cutoff frequency and using the output of this low-pass filter as the reference voltage. If the cutoff frequency is low enough, the output of the low-pass filter will approximate the dc offset of V_{env}. This allows the system to adapt to changing dc offsets and amplitudes while still producing a reliable digital data signal.

In order to achieve a low cutoff frequency, we used the G_m-C filter shown in Fig. 5. The cutoff frequency for this filter is given by

$$f_{-3\ \mathrm{dB}} = \frac{G_m}{2\pi C} \tag{1}$$

where

$$G_m = \frac{\kappa_{\mathrm{eff}} I_{bl}}{2U_t}. \tag{2}$$

I_{bl} is the bias current of the filter, U_T is the thermal voltage kT/q, and κ_{eff} is given by

$$\kappa_{\mathrm{eff}} = \frac{\kappa^2}{\kappa + 1} \tag{3}$$

where κ is the subthreshold gate-coupling coefficient. In modern CMOS processes κ is approximately 0.7. Choosing a bias current I_{bl} of 5 nA and using a 10 pF capacitor gives a calculated cutoff frequency of 459 Hz.

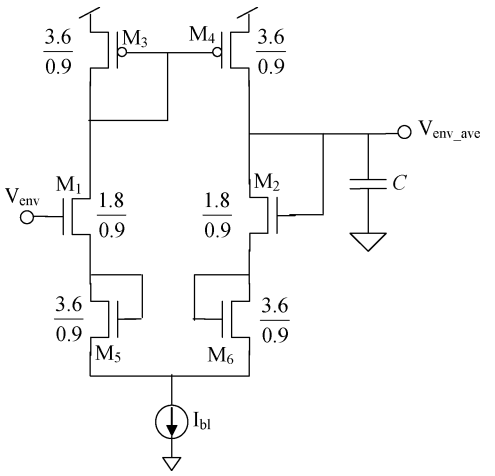

Fig. 5. Schematic of the G_m-C filter. All dimensions are in microns. C = 10 pF.

The final component of the data recovery circuit is the comparator shown in Fig. 6. The two inputs to the comparator are the detected envelope, $V_{\rm env}$, and the average dc value of the detected envelope, $V_{\rm env\_ave}$. The bias current, I_{bc}, was chosen to be 1 μA. The comparator was designed to have approximately 25 mV of hysteresis in order to make the circuit more immune to noise. The output of the comparator is the recovered data signal. Experimental results from this circuit are presented in Section IV.

III. Implantable FM Transmitter

We developed a low-power FM transmitter that operates at 433 MHz. This frequency was chosen because it is the closest short range devices (SRD) band to the FCC-approved Medical Implant Communications Service (MICS) band at 402–405 MHz. The ISM band is suitable for testing and development purposes. The MICS band was established in 1999 and is an ultra-low power, unlicensed radio service for transmitting data in support of diagnostic or therapeutic functions associated with implanted medical devices [17]. This band is divided into 10 channels each having a bandwidth of 300 kHz.

For applications where the antenna is to be positioned directly underneath the skin, such as in this work, tissue absorption can attenuate any RF signal. It has been shown that at 433 MHz, penetration through skin and tissue with high water content has a length constant of 3.57 cm [18]. Thus, transmission from just underneath the skin should be reasonably effective.

As shown in Fig. 7, our low-power transmitter consists of two parts: a neural signal amplifier used to amplify weak signals from an extracellular electrode, and a low-power FM transmitter which transmits the amplified signals outside of the body.

The neural signal amplifier used in this work was previously reported in [19]. It is a fully integrated CMOS circuit having a gain of 40 dB over a 7.5 kHz bandwidth. The amplifier consumes only 52.8 μW of power, and has an input-referred noise of 2.2 μVrms.

An integrated voltage controlled oscillator (VCO) was used as the FM transmitter; in practice, a separate power amplifier was not needed for short-range transmission ($\sim$ 1 m). There are three main architectures for integrated VCOs in use today: the ring oscillator, the Colpitts oscillator, and the fully differential LC-tank oscillator. A transmitter using a Colpitts oscillator has been presented in [20], [14], and a transmitter using a ring oscillator has been presented by [21]. For this project the fully differential LC-tank oscillator was chosen because this type of VCO provides a simple method for producing an FM output while having lower phase noise (frequency jitter) than ring oscillators. The phase noise of the VCO sets the maximum resolution of any FM transmitter.

A schematic of the VCO used in this work is shown in Fig. 8(a). Transistors $\rm M_5$ and $\rm M_6$ act as variable capacitors (varactors) each with a capacitance $2C$ [22]. This capacitance can be varied by changing the voltage $V_{\rm tune}$. R_s is the parasitic series resistance present in the inductor L, representing the finite conductivity of the metal. R_s limits the Q (quality factor) of the inductor. The Q of an inductor is the ratio of imaginary impedance to real impedance, and is given by $Q = (\omega L)/R_s$, where ω is the operating frequency in radians given by $\omega = 1/\sqrt{2LC}$.

It can be shown through small-signal analysis that the incremental input resistance seen when looking into nodes *A* and *B* (ignoring the inductor and capacitors), is given by

$$R_{\rm in} = -\frac{1}{g_m}, \tag{4}$$

where g_m is the transconductance of the transistors $\rm M_1$-$\rm M_4$ and is given by

$$g_m = \sqrt{2\mu C'_{ox} S I_D} \tag{5}$$

where μ is carrier mobility, C'_{ox} is gate oxide capacitance per unit area, S is the transistor width-to-length ratio, and I_D is dc drain current. Devices $\rm M_1$-$\rm M_4$ are sized such that their transconductances are equal.

The circuit in Fig. 8(a) can now be modeled as an incremental resistance of $-1/g_m$ in parallel with an LC tank, as shown in Fig. 8(b). The inductor series resistance, R_s, can be transformed into an equivalent parallel resistance by

$$R_p = R_s\left(Q^2 + 1\right). \tag{6}$$

Fig. 8(b) can be further simplified into the circuit shown in Fig. 8(c), where the resistance R_{eq} is the parallel combination of the negative incremental input resistance, $R_{\rm in}$, and the parasitic parallel resistance of the inductor, R_p. R_{eq} is given by

$$R_{eq} = \frac{-R_{\rm in}R_p}{R_p - R_{\rm in}}. \tag{7}$$

Equation (7) can now be used to establish the requirements for oscillation. From (7), if $|R_{\rm in}| > R_p$, then R_{eq} is positive. A positive R_{eq} has the effect of loading the LC tank, causing the circuit to fall out of oscillation. Conversely, if $|R_{\rm in}| < R_p$, then R_{eq} is negative. When R_{eq} is negative, it no longer loads the LC tank, but instead it supplies power to the LC tank. This condition of having $|R_{\rm in}| < R_p$ allows the VCO to maintain oscillation.

It is interesting to note that from (4) and (5), in order to achieve the required $R_{\rm in}$, either the drain current, I_D, or the width-to-length ratio, S, of the transistors can be changed. That

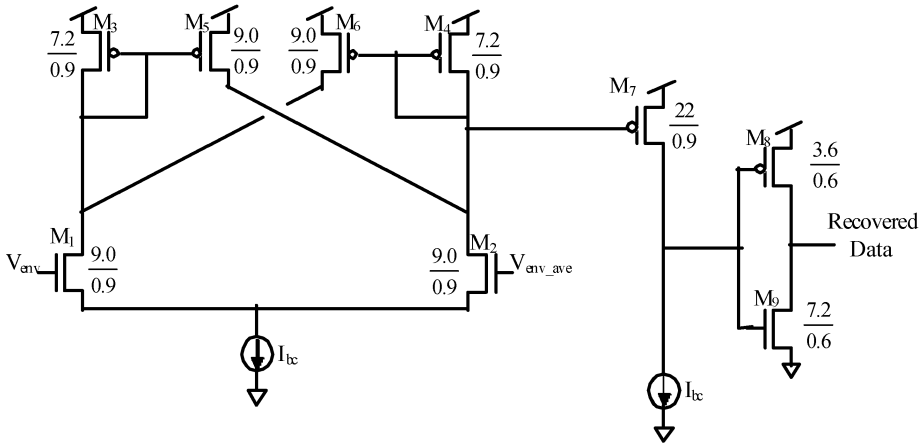

Fig. 6. Circuit schematic of hysteretic comparator. All dimensions are in microns.

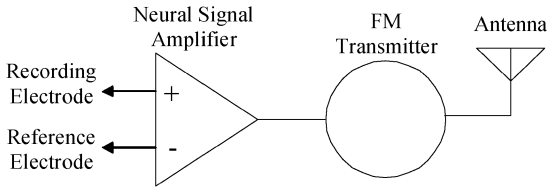

Fig. 7. Block diagram showing the two parts of the implantable transmitter.

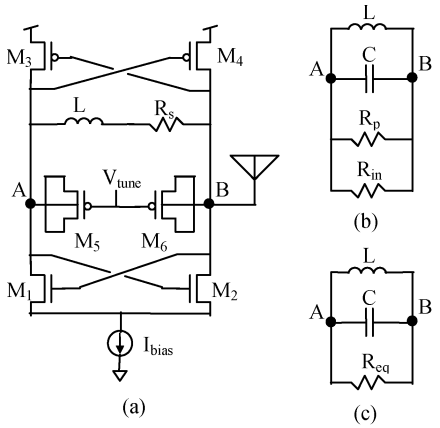

Fig. 8. (a) Schematic of the differential LC VCO used as a transmitter in this work. (b) A simplified model of the VCO shown in (a). (c) A further simplified model used to determine the criterion for oscillation.

is to say, making transistors M_1-M_4 wider can lower the overall power consumption of the transmitter by reducing the required drain current. The disadvantage to this approach is that the parasitic capacitances of the transistors also get larger. This makes the VCO less tunable.

There is yet another way in which the overall power consumption of the VCO can be lowered which does not affect the tunability of the VCO. Note that R_p is directly related to the Q factor of the inductor by (6). This implies that for larger values of Q, a larger R_{in} can be tolerated and still sustain oscillations. Being able to tolerate a larger R_{in} results in a lower g_m, and for a fixed transistor size, a lower drain current can be used. This approach has the advantage of maintaining an acceptable level of tunability in the VCO while allowing for lower power consumption.

To investigate this effect further, (5) and the condition for oscillation established by (7) can be used to derive an expression relating the minimum bias current required to sustain oscillations to the Q factor of the inductor. This is given by

$$I_{b\,\min} = \frac{Q^2}{\mu C_{ox} S\left(\omega L\right)^2 \left(Q^2+1\right)^2}. \tag{8}$$

Fig. 9 shows (8) plotted on a logarithmic scale. Integrated (on-chip) inductors typically have Q values of five or less [23], while discrete (off-chip) inductors can have Q values of 20 or more at a frequency of 433 MHz. As seen in Fig. 9, the power dissipation of a VCO using a low-Q integrated inductor can be an order of magnitude larger than that of a VCO using an off-chip inductor with a Q of 20–30.

With the criteria for oscillation known, transistor sizes can now be calculated. The transmitter was fabricated in a commercially available 0.5 μm 3-metal, 2-poly CMOS process. Table I gives the sizes of the transistors shown in Fig. 8(a). The devices were made large enough to reduce the needed bias current while keeping the parasitic capacitances to a reasonable size. The sizes of transistors M_5 and M_6 are calculated from the following equation

$$C_{\max} = AC'_{ox} + 2WC_{ov} \tag{9}$$

where A is the transistor gate area, W is the transistor gate width, and C_{ov} is the overlap capacitance (per unit length) from the gate to the source/drain regions. $C_{\max}$ is the maximum capacitance that transistors M_5 and M_6 can provide. For this paper, we chose $C_{\max} = 0.9$ pF to achieve oscillations at 433 MHz with a small 47 nH ($\pm 2\%$) surface-mount inductor. The inductor has a Q of approximately 20 at 433 MHz and measures 1.6 mm on its longest dimension. The self-resonant frequency of this inductor is 1.3 GHz, well above the desired operating frequency.

The inductor is the only off-chip component in the FM transmitter. By using an inductor with a Q of 20, the calculated minimum bias current required for oscillation is 20 μA. With a 3.3-V power supply, the calculated minimum power dissipation of the VCO and neural signal amplifier is 119 μW. The low-power consumption of the VCO is largely due to the high Q factor of the off-chip inductor.

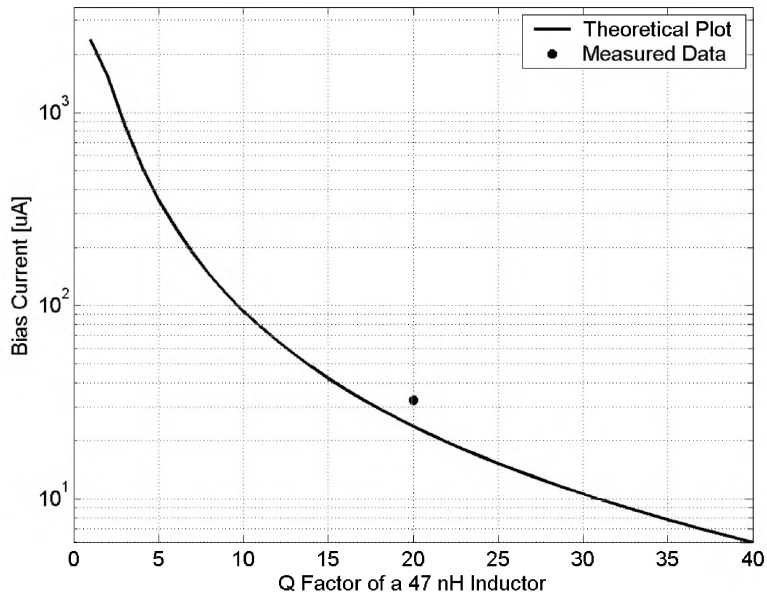

Fig. 9. Plot of VCO bias current $I_{b\,\min}$ versus Q for a 47 nH inductor operating at 443 MHz. The star represents the measured minimum current required by a VCO using a 47 nH inductor with a Q of 20.

TABLE I
VCO TRANSISTOR SIZES

Transistor	Width/Length (μm)
M_1	40.8 / 0.6
M_2	40.8 / 0.6
M_3	81 / 0.6
M_4	81 / 0.6
M_5	630 / 0.6
M_6	630 / 0.6

In order to modulate the 433-MHz carrier signal, the output of the neural signal amplifier was connected to the $V_{\rm tune}$ input of the VCO. Changing this voltage varies the capacitance of M_5 and M_6, which modulates the frequency at which the VCO oscillates.

IV. TESTING AND RESULTS

The clock and data recovery system, neural amplifier, and FM transmitter were fabricated in a 0.5-μm 3-metal, 2-poly CMOS process. The resulting silicon die measured 2.2 mm $\times$ 2.2 mm $\times$ 220 μm, but was packaged in a large (1.5 cm $\times$ 5 cm) 40-pin ceramic package for benchtop testing. In all of the tests described in this section, the circuits were entirely powered using the 1-MHz magnetic link.

A. Clock and Data Recovery Circuit

The overall chip area consumed by the clock and data recovery circuitry was 470 μm$\times$ 390 μm. The measured power consumption of the complete clock and data recovery circuitry was 129 μW. It is important to note that 86% of this power is due to the 110.3 μW dissipated by the two resistors in the prefilter. This power consumption can be lowered by using more chip area to build higher-valued resistors.

In order to test the clock and data recovery circuitry, the transmitted 1-MHz power waveform was amplitude modulated at 1 kHz. Fig. 10(a) shows the class E switch voltage of the power transmitter and Fig. 10(b) shows the recovered on-chip data signal. Fig. 11(a) shows three cycles of the transmitted power waveform, while Fig. 11(b) shows the recovered clock signal. The recovered clock signal has a 50% duty cycle even though the power waveform clearly does not have a 50% duty cycle.

This method of recovering a clock and a data signal from the received power waveform compares favorably to related work. The power consumption of the circuits detailed in this work is only 27% of the power consumption of the clock and data recovery circuitry reported by [24]. The maximum data rate we were able to transmit was 40 kbit/s.

B. FM Transmitter

Fig. 12 shows a microphotograph of the VCO. The overall chip area consumed by the VCO was 117 μm$\times$ 76.5 μm. The total area consumed by the VCO combined with one neural signal amplifier was 94 μm$\times$ 510 μm. The area consumed by the off-chip inductor was 1.6 mm $\times$ 0.8 mm. For all measurements, the circuit was powered from the transcutaneous power link discussed in Section II.

In order to validate (8), we measured the minimum bias current needed to sustain oscillation. We found that 32 μA was the minimum current needed for our VCO using a 47 nH inductor with a Q of 20. This measurement is plotted in Fig. 9 as an asterisk. The measured point falls within 25% of the theoretical line. The measured minimum power dissipation for the VCO and neural signal amplifier was 159 μW, which is in close agreement with the calculated value.

Fig. 13 shows the output frequency of the VCO plotted against the voltage $V_{\rm tune}$. The center frequency of the VCO was measured to be 454 MHz. The maximum variation achievable in the output frequency of the VCO was 26.8 MHz, with a minimum frequency of 440 MHz and a maximum frequency of 466.8 MHz. Because of

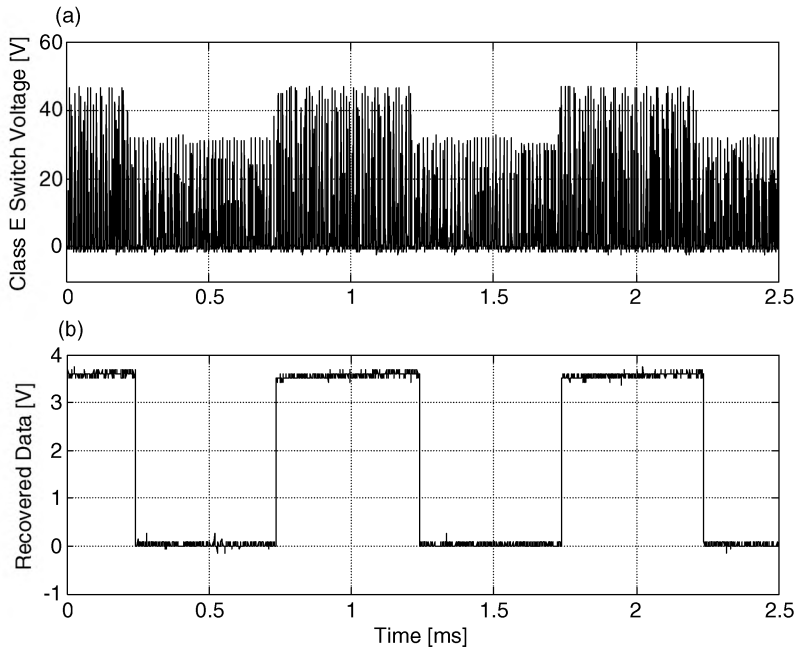

Fig. 10. (a) Switch voltage of the power transmitter showing a 1 kHz square wave modulated onto the transmitted power waveform. (b) The recovered data signal.

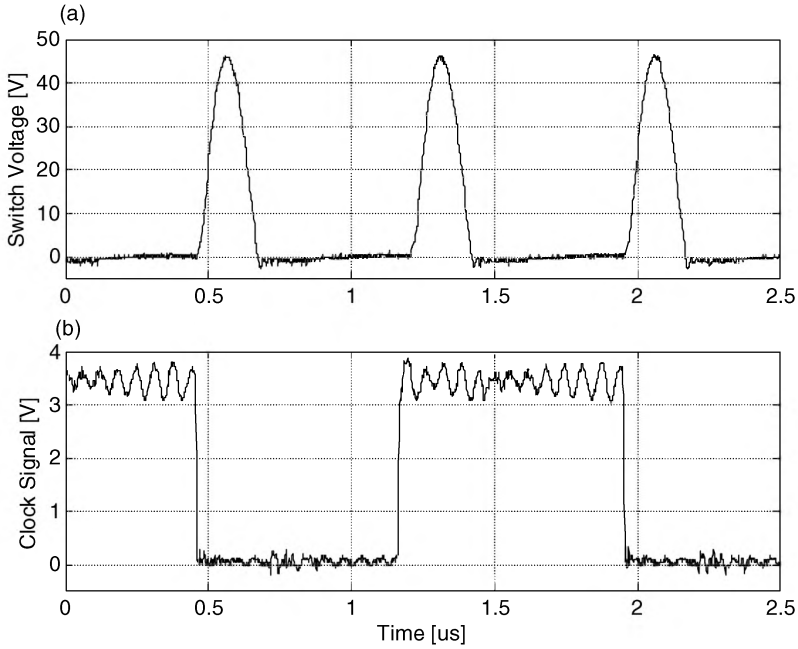

Fig. 11. (a) Three cycles of the transmitted power waveform. (b) The recovered clock signal.

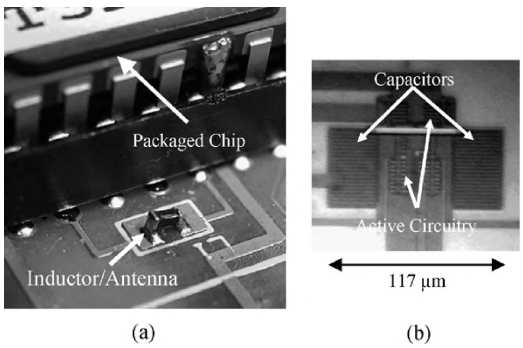

Fig. 12. (a) Photograph of the external inductor that was used as the 0.002λ transmitting antenna. The inductor is 1.6 mm on its longest dimension. (b) Microphotograph of the integrated VCO.

the slight offset in the output frequency, the operating frequency was set to 443 MHz for the remaining measurements.

Note that the output frequency increases, reaches a maximum value, and then decreases. This implies that the varactors are decreasing in value, reaching a minimum capacitance, and then increasing back toward their initial values. This behavior is typical in the presence of a low frequency signal (typically below 100 Hz) [25]. It is due to the source and drain regions in the MOS varactors that we observe this behavior in the presence of a 443-MHz signal. The source and drain regions are large reservoirs of minority carriers and are capable of supplying/receiving the extra minority carriers at a much faster rate than the usual methods of thermal generation and recombination [22].

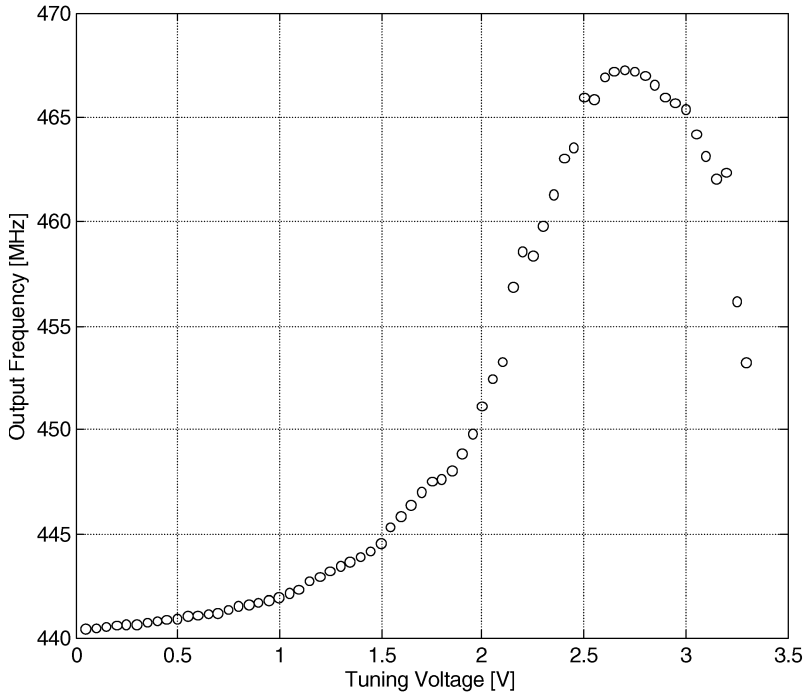

Fig. 13. Output frequency of the VCO versus the tuning voltage.

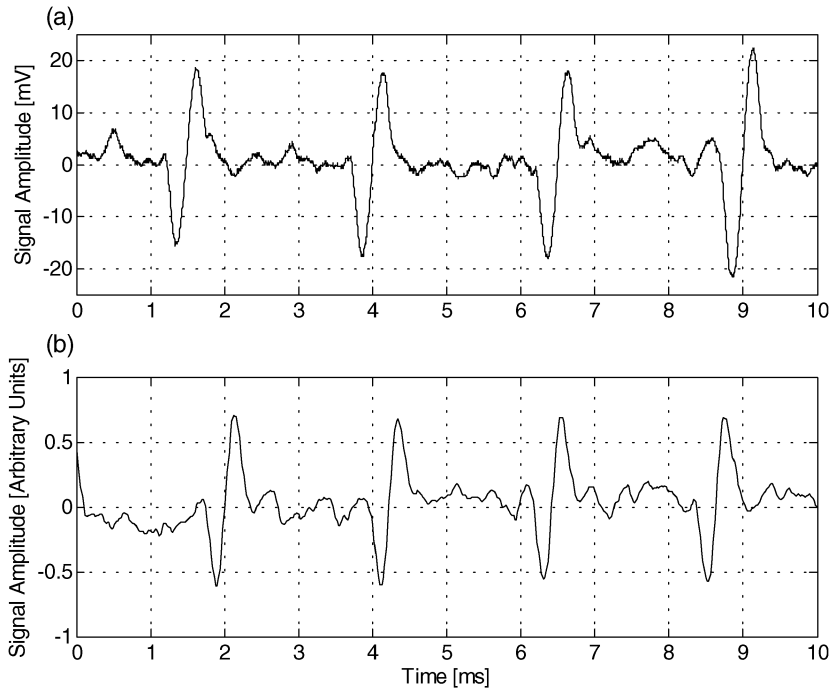

Fig. 14. (a) The output of the neural signal amplifier (gain $= 100$). (b) The demodulated, received waveform after being transmitted a distance of 1 m.

The phase noise of the VCO was measured using the phase noise personality installed on an Agilent E4402B 3-GHz spectrum analyzer. The phase noise at an offset of 300 kHz from the carrier was measured to be -96.8 dBc/Hz. The transmitter was then tested using the off-chip inductor as the antenna [see Fig. 12(a)]. This is equivalent to using a 0.002λ antenna. The bias current for the VCO was increased to 125 μA in order to obtain the desired transmission range and received power levels. The current consumed by the neural signal amplifier was 16 μA. This resulted in a measured power consumption of 465 μW at a supply voltage of 3.3 V.

To simulate extracellular neural signals, a single cycle of a 225 μV amplitude sine wave with a period of 0.53 ms was repeated every 2.5 ms. This signal was applied to the input of the neural signal amplifier. The receiver, a WinRadio 3150E FM receiver with a 30.5-cm monopole antenna, was placed one meter away from the transmitter. Fig. 14 shows the received waveform plotted with the output of the neural signal amplifier.

The WinRadio is an uncalibrated receiver; hence, the amplitude of the received waveform is in arbitrary units. Furthermore, our measurement equipment did not allow us to take simultaneous measurements of the transmitted and received data and,

hence, the measurements were taken manually at two separate times.

The received power was measured using an Agilent E4402B spectrum analyzer with a 30.5-cm monopole antenna attached to its input. With the longest dimension of the transmitting antenna parallel to the receiving antenna the received power was measured to be -59.73 dBm. The orientation of the transmitting antenna was then changed so that its longest dimension was normal to the receiving antenna, the received power dropped to -63.41 dBm. Finally, when the transmitting antenna was pointing directly at the receiving antenna, the received power was measured to be -75 dBm. This was only slightly above the noise floor of the measurement equipment, which was -85 dBm.

The primary advantage of this circuit is its low-power consumption. The transmitter consumes only 25% of the 2 mW consumed by the circuit in [5], 6.8% of the 6.8 mW consumed by the circuit in [4], and only 4.7% of the 10 mW consumed by the transmitter reported in [3]. The transmission range of this work, however, is only 1 m, whereas the transmission range of [5] is 2 m and 15 m for [3]. No transmission range was reported for [4]. For the types of applications that this transmitter is intended, it will only need to transmit 1 m (e.g., to a receiver located on a patient's body).

V. Conclusions

We have presented a bidirectional telemetry system that is capable of being entirely powered from a magnetic transcutaneous link. A low-power, integrated circuit for reconstructing a clock and a data signal from the power waveform was also presented. The clock recovery circuit is capable of generating a digital clock signal with a 50% duty cycle regardless of the duty cycle of the received power waveform. The data recovery circuit robustly recovers a data signal that has been amplitude modulated onto the transmitted power waveform. The power consumption of the clock and data recovery circuitry was measured to be 129 μW.

We presented an implantable FM transmitter that dissipates only 465 μW of power. It was demonstrated that this transmitter can successfully transmit data distances of up to one meter while being powered from a magnetic transcutaneous link and using only a small off-chip inductor as an antenna. The results demonstrate the feasibility of using a micropower transmitter in a fully implantable neural recording system. While we have demonstrated FM transmission of a single analog waveform, additional neural waveforms could be transmitted by adding a multiplexer to the system. If digital transmission is preferred, an analog-to-digital converter could be used along with digital FSK transmission using the same low-power transmitter. As a next step, this system should be evaluated using skin or an effective skin surrogate between the transmitter and receiver to measure attenuation in a realistic implanted situation.

Our current VCO design relies on capacitors and an inductor to set the transmission frequency. Capacitance and inductance values typically exhibit a weak temperature dependence, and can vary by 10% or more from one device to the next. In order to maintain a precise transmitting frequency, future circuits should use a phase-locked-loop-based frequency synthesizer to lock the VCO at some multiple of a precise frequency reference. Precise frequency references typically utilize quartz crystals or SAW oscillators, but these devices cannot be integrated on a CMOS chip. A better source for a reference frequency would be the received power signal, which is set by a precise nonimplanted circuit – the class E transmitter.

We presented a relationship between the Q factor of inductors and the overall power dissipation of a VCO. We see that a relatively high-Q inductor is necessary for low-power operation. While an off-chip inductor was chosen for this project, the Q value of integrated inductors can be increased by using MEMS postprocessing steps such as etching away the substrate underneath the inductor [23] or using a VLSI process optimized for high-Q RF inductors. Future implantable transmitters should take advantage of this technology to achieve the smallest possible size and power consumption.

An important issue not explicitly addressed in this work is possible interference caused by the strong ac magnetic field used to power the implantable device. In our system, the transmitting and receiving coils were placed approximately 10–20 cm from the electronics, and we observed no effect of the power signal on the VCO or the neural signal amplifier. Further tests should be done with the coils directly over the integrated electronics to determine if interference due to magnetic coupling poses a problem in compact implanted systems.

References

[1] C. T. Nordhausen, E. M. Maynard, and R. A. Normann, "Single unit recording capabilities of a 100-microelectrode array," *Brain Res.*, vol. 726, pp. 129–140, 1996.

[2] A. C. Hoogerwerf and K. D. Wise, "A three-dimensional microelectrode array for chronic neural recording," *IEEE Trans. Biomed. Eng.*, vol. 41, no. 12, pp. 1136–1146, Dec. 1994.

[3] S. Takeuchi and I. Shimoyama, "A radio-telemetry system with a shape memory alloy microelectrode for neural recording of freely moving insects," *IEEE Trans. Biomed. Eng.*, vol. 15, no. 1, pp. 133–137, Jan. 2004.

[4] E. A. Johannessen, L. Wang, L. Cui, T. B. Tang, M. Ahmadian, A. Astaras, S. W. J. Reid, P. S. Yam, A. F. Murray, B. W. Flynn, S. P. Beaumont, D. R. S. Cumming, and J. M. Cooper, "Implementation of multichannel sensors for remote biomedical measurements in a microsystems format," *IEEE Trans. Biomed. Eng.*, vol. 51, no. 3, pp. 525–535, Mar. 2004.

[5] P. Mohseni, K. Nagarajan, B. Ziaie, K. Najafi, and S. B. Crary, "An ultralight biotelemetry backpack for recording EMG signals in moths," *IEEE Trans. Biomed. Eng.*, vol. 48, no. 6, pp. 734–737, Jun. 2001.

[6] V. Annovazzi-Lodi and S. Donati, "An optoelectronic interconnection for bidirectional transmission of biological signals," *IEEE Trans. Biomed. Eng.*, vol. 35, no. 8, pp. 595–606, Aug. 1988.

[7] S. Kawahito, S. Ueda, M. Ishida, T. Nakamura, S. Usui, and S. Nagaoka, "A CMOS integrated circuit for multichannel multiple-subject biotelemetry using bidirectional optical transmissions," *IEEE Trans. Biomed. Eng.*, vol. 41, no. 4, pp. 400–406, Apr. 1994.

[8] B. Ziaie, S. C. Rose, M. D. Nardin, and K. Najafi, "A self-oscillating detuning-insensitive class-E transmitter for implantable microsystems," *IEEE Trans. Biomed. Eng.*, vol. 48, no. 3, pp. 397–400, Mar. 2001.

[9] E. S. Hochmair, "System optimization for improved accuracy in transcutaneous signal and power transmission," *IEEE Trans. Biomed. Eng.*, vol. 31, pp. 177–186, Feb. 1984.

[10] M. Soma, D. C. Galbraith, and R. L. White, "Radio-frequency coils in implantable devices: Misalignment analysis and design procedure," *IEEE Trans. Biomed. Eng.*, vol. BME-34, no. 4, pp. 276–282, Apr. 1987.

[11] P. R. Troyk and M. A. K. Schwan, "Closed-loop class E transcutaneous power and data link for microimplants," *IEEE Trans. Biomed. Eng.*, vol. 39, no. 6, pp. 589–599, Jun. 1992.

[12] C. Charles, "Electrical components for a fully implantable neural recording system," Masters thesis, Univ. Utah, Elect. Comput. Eng. Prog., Salt Lake City, Utah, 2003.

[13] M. Ghovanloo and K. Najafi. "Fully integrated wideband high-current rectifiers for inductively powered devices." *IEEE J. Solid-State Circuits*. vol. 39. no. 11. pp. 1976–1984. Nov. 2004.
[14] P. R. Troyk and G. A. DeMichele. "Inductively-coupled power and data link for neural protheses using a class-E oscillator and FSK modulation." in *Proc. 2003 Int. Conf. IEEE Engineering in Medicine and Biology Society*. Cancún. Mexico. Sep. 2003. pp. 3028–3031.
[15] W. Liu. K. Vichienchom. M. Clements. S. C. DeMarco. C. Hughes. El McGucken. M. S. Humayun. E. de Juan. J. D. Weiland. and R. Greenberg. "A neuro-stimulus chip with telemetry unit for retinal prosthetic device." *IEEE J. Solid-State Circuits*. vol. 35. no. 10. pp. 1487–1497. Oct. 2000.
[16] C. Mead. *Analog VLSI and Neural Systems*. Reading. MA: Addison-Wesley. 1989.
[17] About Medical Implant Communications. Federal Communications Commission. [Online]. Available: http://wireless.fcc.gov/services/personal/medicalimplant/about/
[18] C. C. Johnson and A. W. Guy. "Nonionizing electromagnetic wave effects in biological materials and systems." *Proc. IEEE*. vol. 60. no. 6. pp. 692–718. Jun. 1972.
[19] R. R. Harrison and C. Charles. "A low-power low-noise CMOS amplifier for neural recording applications." *IEEE J. Solid-State Circuits*. vol. 38. no. 6. pp. 958–965. Jun. 2003.
[20] M. Ahmadian. B. W. Flynn. A. F. Murray. and D. R. S. Cumming. "Miniature transmitter for implantable micro systems." in *Proc. 2003 Int. Conf. IEEE Engineering in Medicine and Biology Society*. Cancún. Mexico. Sep. 2003. pp. 3028–3031.
[21] G. A. DeMichele and P. R. Troyk. "Integrated multi-channel wireless biotelemetry system." in *Proc. 2003 Int. Conf. IEEE Engineering in Medicine and Biology Society*. Cancún. Mexico. Sep. 2003. pp. 3372–3375.
[22] A. Porret. T. Melly. C. C. Enz. and E. A. Vittoz. "Design of high-q varactors for low-power wireless applications using a standard CMOS process." *IEEE J. Solid-State Circuits*. vol. 35. no. 3. pp. 337–345. Mar. 2000.
[23] A. Rofourgan. J. Rael. M. Rofourgan. and A. Abidi. "A 900-MHz CMOS LC-oscillator with quadrature outputs." in *ISSCC Dig. Tech. Papers*. San Francisco. CA. Feb. 1996. pp. 392–393.
[24] H. Yu and K. Najafi. "Circuitry for a wireless microsystem for neural recording microprobes." in *Proc. 2001 Int. Conf. IEEE Engineering in Medicine and Biology Society*. Istanbul. Turkey. Oct. 2001. pp. 761–764.
[25] S. M. Sze. *Semiconductor Devices: Physics and Technology*. New York: Wiley. 2002.

Nathan M. Neihart (S'02) was born in Salt Lake City. Utah. in 1979. He received both the B.S. and M.S. degrees in electrical engineering from the University of Utah. Salt Lake City. in 2004. His thesis involved designing circuits for wireless bidirectional data transfer in neural recording applications. He is currently working toward the Ph.D. degree in electrical engineering at the University of Washington. Seattle.

Reid R. Harrison (S'98–M'00) received the B.S. degree in electrical engineering from the University of Florida. Gainesville. in 1994 and the Ph.D. degree in computation and neural systems from the California Institute of Technology. Pasadena. in 2000.

He joined the University of Utah. Salt Lake City. in 2000. where he is now an Assistant Professor of Electrical and Computer Engineering and an Adjunct Assistant Professor of Bioengineering. He has over 30 refereed publications since 1999 in the fields of low-power analog and mixed-signal CMOS circuit design. integrated electronics for neural interfaces and other biomedical devices. and hardware for biologically inspired computational systems.

Dr. Harrison organized the 2001 IEEE SSCTC Workshop on Low-Power Circuits in Arlington. VA. He received the National Science Foundation CAREER Award in 2002.